# Photoelectron Imaging of Cells: Photoconductivity Extends the Range of Applicability

Douglas L. Habliston,* Karen K. Hedberg,* G. Bruce Birrell,* Gertrude F. Rempfer,‡ and O. Hayes Griffith*
*Institute of Molecular Biology and Department of Chemistry, University of Oregon, Eugene 97403-1229, and ‡Department of Physics, Portland State University, Portland, Oregon 97207-0751 USA

ABSTRACT Photoelectron imaging is a sensitive surface technique in which photons are used to excite electron emission. This novel method has been applied successfully in studies of relatively flat cultured cells, viruses, and protein-DNA complexes. However, rounded-up cell types such as tumor cells frequently are more difficult to image. By comparing photoelectron images of uncoated and metal-coated MCF-7 human breast carcinoma cells, it is shown that the problem is specimen charging rather than a fundamental limitation of the electron imaging process. This is confirmed by emission current measurements on uncoated monolayers of MCF-7 carcinoma cells and flatter, normal Wi-38 fibroblasts. We report here that sample charging in photoelectron microscopy can be eliminated in most specimens by simultaneous use of two light sources—the standard UV excitation source (e.g., 254 nm) and a longer wavelength light source (e.g., 325 nm). The reduction in sample charging results largely from enhanced photoconduction in the bulk sample and greatly extends the range of cells that can be examined by photoelectron imaging. The contributions of photoconductivity, the electric field of the imaging system, and the short escape depths of the photoelectrons combine to make photoelectron imaging a uniquely sensitive technique for the study of biological surfaces.

## INTRODUCTION

It is becoming increasingly evident that many important events occur on the surfaces of mammalian cells. For example, specific receptors at the cell surface mediate cellular adhesion, initiate signal transduction cascades, and are involved in the generation of matrix-degrading enzymes and alterations that permit invasion of normal tissue by malignant tumor cells (Clark and Brugge, 1995; Sheetz, 1995; Danø et al., 1994). Imaging cell surfaces is an important aspect of characterizing these processes, but it is a challenging goal, because the plasma membrane is thin, delicate, and heterogeneous. The photoelectric effect provides the fundamental physical basis of a family of techniques that have unique advantages for studying surfaces. These methods are based on Einstein's equation,

$$KE = h\nu - \phi \quad (1)$$

where $h\nu$ is the energy of the exciting light, $\phi$ is the work function or binding energy that must be overcome, and $KE$ is the kinetic energy of the emitted electron. There is a wealth of information carried by the electrons, including the point where the electrons leave the surface, the escape depth, kinetic energy, energy spread, and even the angular distribution. Instrumentation developments are in progress in many laboratories, each designed to optimize one type of information about surfaces, including semiconductors and catalytic surfaces as well as cell surfaces (Griffith and Engel, 1991). The developments may be classified as either parallel imaging (utilizing lenses) or sequential imaging (utilizing scanning photon beams). Instruments that optimize the $KE$ information to obtain elemental distributions are called spectromicroscopes, x-ray secondary emission microscopes, or x-ray photoelectron microscopes, and utilize high-energy x-ray photons from conventional x-ray sources or synchrotron radiation to eject core electrons (Tonner and Harp, 1988; De Stasio and Margaritondo, 1994; Holldack and Grunze, 1994). An imaging instrument equipped with UV light ejects only valence electrons. The most advanced instrument of this type is called a photoelectron microscope (PEM) or a photoelectron emission microscope (PEEM) (reviewed in Griffith and Engel, 1991). These various approaches are not mutually exclusive and some instruments can be equipped with either soft x-ray sources or UV light.

It should be noted that spatial resolution, energy resolution, and signal intensity are interrelated features in photoelectron imaging. If the goal is elemental analysis, higher excitation energies are required because core electrons are ejected. The accompanying spread in electron energies results in increased chromatic aberrations, whereas the use of energy analysis decreases signal intensity. These factors compromise the spatial resolution desired in a technique where sample imaging is the primary intent. We have been involved in an effort to maximize spatial resolution, with the goal of obtaining macromolecular resolution on biological specimens (Birrell et al., 1994; Hedberg et al., 1994; Rempfer and Griffith, 1992; Habliston et al., 1986). To achieve this goal, we have concentrated on the relatively low excitation energies provided by UV light, i.e., "threshold illumination" in a parallel imaging mode (i.e., PEM/PEEM, Fig. 1). In this approach, only valence electrons are ejected from the surface, and the spread in kinetic energies of the emitted electrons is small.

*Received for publication 30 May 1995 and in final form 14 July 1995.*

Address reprint requests to O. Hayes Griffith, Institute of Molecular Biology, University of Oregon, Eugene, OR 97403-1229. Tel: 503-346-4634; Fax: 503-346-4643; E-mail: hayes@image1.uoregon.edu.



0006-3495/95/10/1615/10 $2.00

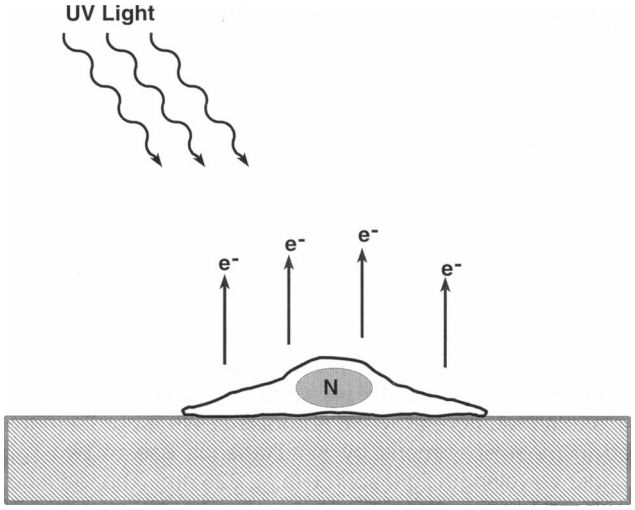


FIGURE 1 Diagram of photoelectron emission from a cultured cell. In photoelectron microscopy the imaging is carried out in the parallel mode rather than with scanning. The specimen is placed on the cathode, and the low-energy electrons are then accelerated in an electric field between the cathode and anode, and the image is magnified by an electron lens system similar to that of a transmission electron microscope (TEM). Unlike the TEM, the photoelectron microscope has no electron gun. The specimen itself is the source of the electrons.

PEM can be described as the electron optical analogue of fluorescence microscopy, and these two techniques are being applied in molecular and cell biology in a complementary manner. Both techniques use UV light to illuminate the specimen and stimulate a signal. Both techniques utilize immunolabeling in place of elemental analytical data. The lateral resolution in PEM is much higher (i.e., 5–10 nm) than in fluorescence microscopy, because the wavelength of the emitted electron is much shorter than that of the emitted light. PEM also has very high topographic contrast, because the specimen is in an electric field, which influences the trajectories of the low-energy electrons as they leave the cell surface. This makes it possible to see fine surface detail in PEM, but it also places a limitation on the amount of surface relief that can be imaged without distortions. During the course of studies of cultured cells, we observed that tumor cells are often more difficult to image by PEM than the typically well-spread "normal" fibroblasts and epithelial and endothelial cells that have been successfully imaged previously (Birrell, et al., 1991; Habliston et al., 1986). Tumor cells tend to exhibit more rounded morphology and often have a much more pronounced topography than normal attached cells in culture. The question arises: Is specimen charging responsible for the image artifacts, or is the morphology of these cells exceeding the limit that can be imaged in the present PEM? To distinguish between these two possibilities, we undertook the biophysical study reported here. In addition to identifying the problem as specimen charging, a solution is proposed and tested. An analysis of the specimen charging and the role of photoconductivity is presented that is relevant to all forms of photoelectron imaging.

## MATERIALS AND METHODS

### Cell culture

The MCF-7 human breast carcinoma cell line, human glioma lines H4 and SW1088, human adenocarcinoma line SW13, and Wi-38 normal human lung fibroblasts were obtained from the American Type Culture Collection (Rockville, MD). Cells were routinely cultured in DME medium (Celox Corp., Hopkins, MN) with the addition of 10% iron-enriched calf serum (Intergen, Purchase, NY). For observation by PEM, these cells were seeded either alone or together onto 5-mm chromium-coated glass microscope coverslips. After 2–3 days in culture, the coverslip samples to be examined without labeling were washed twice in phosphate-buffered saline (PBS, Celox) and fixed in 2% EM grade glutaraldehyde (Polysciences, Warrington, PA) in 0.1 M Na cacodylate, pH 7.4. Samples were stored (typically 1–5 days) at 4°C in fixative until further processing for PEM.

### Specimen preparation for photoelectron microscopy

Glutaraldehyde-fixed coverslip cultures of cells were postfixed in 1% $OsO_4$ in 0.05 M cacodylate buffer for 1–2 h at room temperature in the dark. After washing extensively in deionized water the samples were either dehydrated through a graded series of concentrations of ethanol in water followed by critical point drying from $CO_2$, or by cryofixation followed by freeze substitution (Ryan, 1992). For the latter, the sample disk was mounted on the modified vacuum chuck of a "Gentleman Jim" quick-freezing apparatus (A. F. Boyne, Friday Harbor, WA). The sample was lightly blotted to remove excess surface water, then plunged into liquid $N_2$-cooled ethane. This procedure eliminates any heat load from the sample carriage hardware. The frozen sample was then transferred to acetone at −80°C with cooled forceps to allow substitution of water for 24 to 72 h. After rinsing in cold fresh acetone the samples were freeze-dried using liquid $N_2$-cooled sorb pumps. Dehydrated samples were stored at $10^{-8}$ Torr in the oil-free preparation chamber of the PEM until examination.

A few samples were coated with a thin layer of conductive Pt/Pd before examination in the PEM. This was done in an oil-free high-vacuum resistance source evaporator equipped with an Inficon XTM quartz crystal oscillator thickness monitor to control the Pt/Pd layer thickness. The samples were mounted on a goniometer stage to provide control of the angle of deposition.

### Photoelectron imaging of cells

The oil-free, high-vacuum photoelectron microscope for biological work is described elsewhere (Rempfer et al., 1991). The 5-mm-diameter chromium-coated glass microscope coverslip (no. 1 thickness), on which the specimen was grown, is mounted on the end of a specimen rod and held in place by a small metal collar. The coverslip is placed in the cathode support structure, and the microscope is evacuated. The high-voltage power supply and the UV light are then switched on. The emitted photoelectrons are accelerated by a 30-kV voltage differential between the cathode and anode, and then imaged with an electrostatic electron lens system. The final magnified image is projected onto either electron image film (Kodak SO-163) or an aluminum-coated phosphor screen on a fiber optic window. When the window is used, the output is fiber-optically coupled to either a cooled integrating CCD or an intensified CCD video camera. Beam current measurements are made by collecting the current on the aluminum-coated phosphor screen connected to a Keithley Instruments (Cleveland, Ohio) model 26000 picoammeter. This arrangement allows simultaneous beam current data collection and visual observation. To produce the photoemission, the specimen is typically illuminated by UV light from one or two HBO 100 W/2 high-pressure short arc Hg vapor lamps with

quartz envelopes. UV light from each arc lamp is focused onto the sample by means of two aspheric $MgF_2$ lenses (Janos Technology, Townshend, VT), one of which is fixed at the focal distance from the specimen inside the evacuated microscope column. The other lens of the aspheric pair is mounted inside a water-cooled housing on a micrometer controlled carriage outside the vacuum chamber. An infrared-blocking water cell separates this lens from the Hg arc lamp. The micrometer control of the lens carriage is adjusted to indexed positions to provide a measure of focal isolation, i.e., to illuminate the sample with wavelength bands covering the spectrum of the Hg arc lamp. The actual wavelength band reaching the sample surface was determined with a Bausch and Lomb model 33-86-07 monochromator. Emission scans corresponding to each lens index position of the Hg lamp light source were recorded using a photometer with a 300–650 nm photomultiplier tube and a sodium salicylate-coated entrance window. Focal isolation does not separate wavelengths as completely as a monochromator, but it provides the greater photon flux desired for microscopy. For example, adjusting the aspheric optics for short wavelength passes the broad 250–270 nm Hg band (i.e., the region around the 254 nm line) but also passes part of the longer wavelength light. Adjusting the optics for long wavelength illumination maximizes the broad 290–320 nm Hg band but likewise passes some of the shorter wavelengths. Alternatively, one of the arc lamps can be replaced by a laser. Here we used either a Liconix (Santa Clara, CA) model 4240NB He/Cd laser, which can be configured for a continuous-wave 15–40 mW multimode beam at either 325 nm or 440 nm, or an Omnichrome (Chino, CA) model 3074-30 m He/Cd 30 mW continuous-wave laser at 325 nm. The beam of laser light is directed onto the sample through a $MgF_2$ vacuum port window. We have avoided pulsed lasers because of space charge effects (Massey et al., 1991).

## RESULTS

### Photoelectron images of uncoated cells with mercury arc lamps

Fig. 2 shows a pair of PEM micrographs taken with two different illumination conditions. The specimen consists of a co-culture of two morphologically different cell types: normal human lung fibroblasts (Wi-38 cells) and human breast carcinoma cells (MCF-7 cells). Normal fibroblasts are typically well spread, fairly flat, and easily imaged by PEM. MCF-7 cells, as with many tumor cell types, are less adherent to the substrate, causing them to be thicker and rounder than normal cells. The result in PEM is that with mercury arc lamp illumination alone, tumor cell types such as MCF-7 can exhibit charging artifacts. The image in Fig. 2 *a* was recorded using one Hg arc lamp, with its aspheric lenses focused to optimize sample illumination from the shorter wavelength UV spectral lines (e.g., 254 nm). This is the standard setting for PEM, as it generates maximum photoemission, and therefore image intensity, from biological samples. In Fig. 2 *a*, the Wi-38 fibroblast at right is clearly imaged, whereas the two tumor cells at left are characterized by dark, blurry areas. Decreasing the amount of UV irradiation striking the sample by shuttering the lamp decreased the overall image brightness but did not reduce the apparent charging at the tumor cell surface. Fig. 2 *b* was recorded with two mercury arc sources: one lamp with its UV lens system optimized for short UV light as before, and the other lens system optimized for longer UV wavelengths (~325 nm and longer). The addition of the longer wavelength illumination dramatically changed the image. The artifacts disappeared, and the MCF-7 tumor cells are well imaged.

### Photoelectron imaging of uncoated cells with laser illumination

The use of focal isolation is rapid and effective, but it amounts to enriching the sample illumination with a range of wavelengths, rather than selectively with a single wavelength. To illuminate the specimen with light of well-defined long wavelength, one of the Hg arc lamps was replaced with a He/Cd laser with output at 325 nm. Fig. 3 illustrates images of MCF-7 cells with one Hg arc lamp

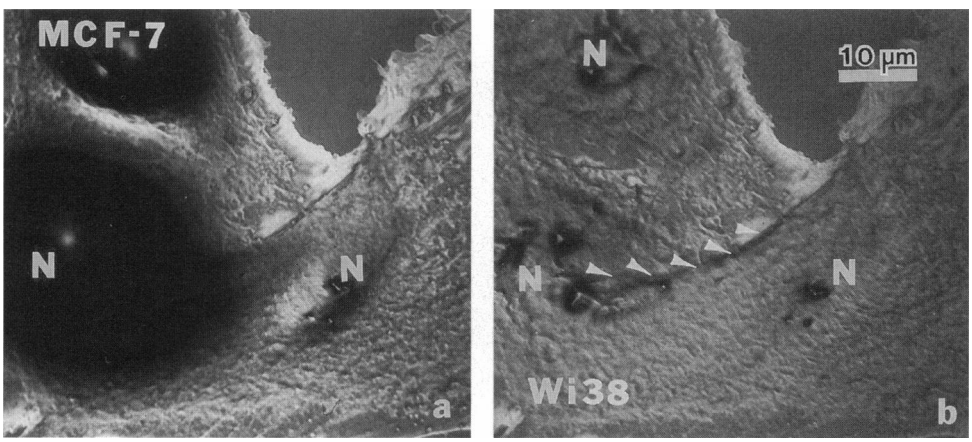


FIGURE 2 Co-culture of MCF-7 human breast carcinoma cells and Wi-38 normal human lung fibroblasts (labeled MCF and Wi-38, respectively). (*a*) Photograph illustrating a common problem encountered in photoelectron imaging of cultured cells with conventional UV lamp excitation (254 nm). The flatter Wi-38 cells produce good images, whereas rounder and thicker MCF-7 cells show artifacts (dark areas on far left). (*b*) These artifacts are eliminated by switching on a second Hg arc lamp with lenses tuned to illuminate the sample with the longer UV wavelength bands (>300 nm). With two wavelength illumination, it can easily be seen that the two MCF-7 cells are in the process of invading beneath the Wi-38 fibroblast. The nucleus (Nu) of the lower MCF-7 cell is half covered by the fibroblast, and in that region the edge of the fibroblast is indicated by arrowheads. The dark flat area near the top center of each photograph is the exposed substrate.

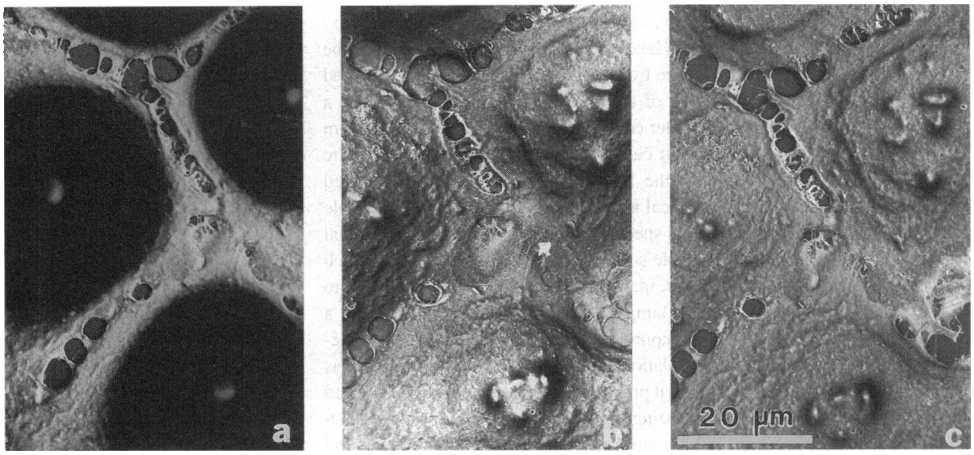


FIGURE 3 Gross charging artifact observed in a field of uncoated MCF-7 cancer cells (*left*), eliminated by means of a combination of illumination sources. (*a*) Hg arc lamp alone, with lenses focused to illuminate the sample with short wavelengths (~254 nm); (*b*) Liconix He/Cd laser only (325 nm); (*c*) combined laser and arc lamp illumination. Actual exposure times were 14 s, 100 s, and 7 s, respectively, to provide similar overall brightness.

only, set to the short wavelength range (Fig. 3 *a*); with the 325 nm laser only (Fig. 3 *b*); and with these two light sources combined (Fig. 3 *c*). In Fig. 3 *a*, as in Fig. 2 *a*, the arc lamp alone permits detailed observation of only the peripheries of the cells while the nuclei appear as dark regions. The image obtained with the laser alone (Fig. 3 *b*) required an approximately 10-fold longer exposure time because of the lower emission current of photoelectrons, but shows a clearly resolved nuclear region. Combining the two light sources allowed an exposure time comparable to that obtained with the Hg arc lamps, but without the charging artifacts (Fig. 3 *c*). The effects were reversible; that is, charging reappeared immediately when the laser was turned off. The same effects were replicated with several additional tumor cell lines, including the human glioma lines SW1088 and H4, and human adenocarcinoma SW13 (not shown). Similar results were obtained using the He/Cd laser with mirrors configured to transmit the 440-nm wavelength line. The 440-nm line eliminated the charging artifacts when used in combination with the arc lamp but produced no measurable photoemission when used alone.

## Photoelectron imaging of metal-coated cells

A culture of MCF-7 cells was prepared and coated with a thin layer (~2 nm) of platinum-palladium and examined with short-wavelength UV illumination (Fig. 4). The photoelectron micrograph of the metal-coated cell surface is well resolved and exhibits none of the dark, fuzzy regions characteristic of images of uncoated MCF-7 cells obtained with short-wavelength illumination alone. This confirms that the image artifacts are not due to specimen topography.

## Photoelectron imaging of cells with aperture adjusted to enhance 3D effect

Fig. 5 is a good example of what can be achieved in photoelectron imaging of cultured cells with two UV wavelength bands, one for excitation and the other for photoconduction. This is a larger field of view of the same MCF-7 human breast carcinoma cell culture as in Fig. 3. These cells are not coated with metal, as is done in conventional scanning electron microscopy. One complete cell and parts of five other cells are shown. The smooth, dark area in the lower left-hand corner and between cells is the substrate. Topographical features can be highlighted by adjusting the aperture to slightly off-center to enhance the three-dimensional effect characteristic of PEM images, as illustrated in this micrograph. The complex texture of these uncoated cell surfaces is readily visible, as are the more obvious landmarks of the large nuclei and the nucleoli contained within them. When grown on a solid substrate such as a coverslip or PEM sample mount, MCF-7 cells spread outward on the surface as expanding "colonies" of cells. Nevertheless, the individual carcinoma cells do not form the tight cell-cell contacts typical of normal epithelial cells in a confluent monolayer, and the large gaps between cells are very evident in Fig. 5. Specimen shrinking during critical point drying is a contributing factor but is not the main cause,

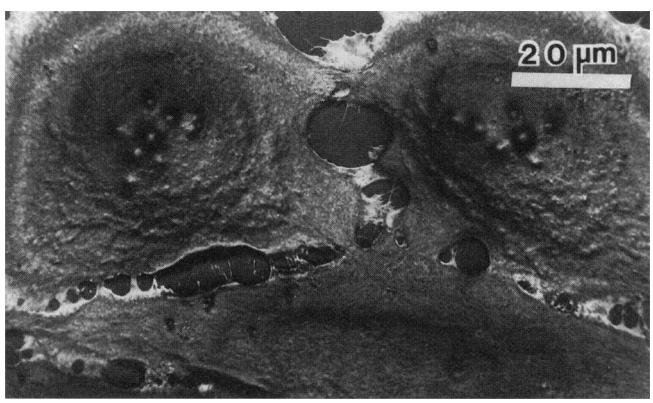


FIGURE 4 Photoelectron micrograph of a metal-coated cell. An MCF-7 culture similar to that of Fig. 3 was coated with approximately 2 nm of platinum-palladium, the image was recorded during illumination with one Hg arc lamp, and the optics were optimized for short wavelengths. Exposure time of the original negative was 0.6 s. Other than overall brightness, the image did not change significantly with changes in illumination wavelength.

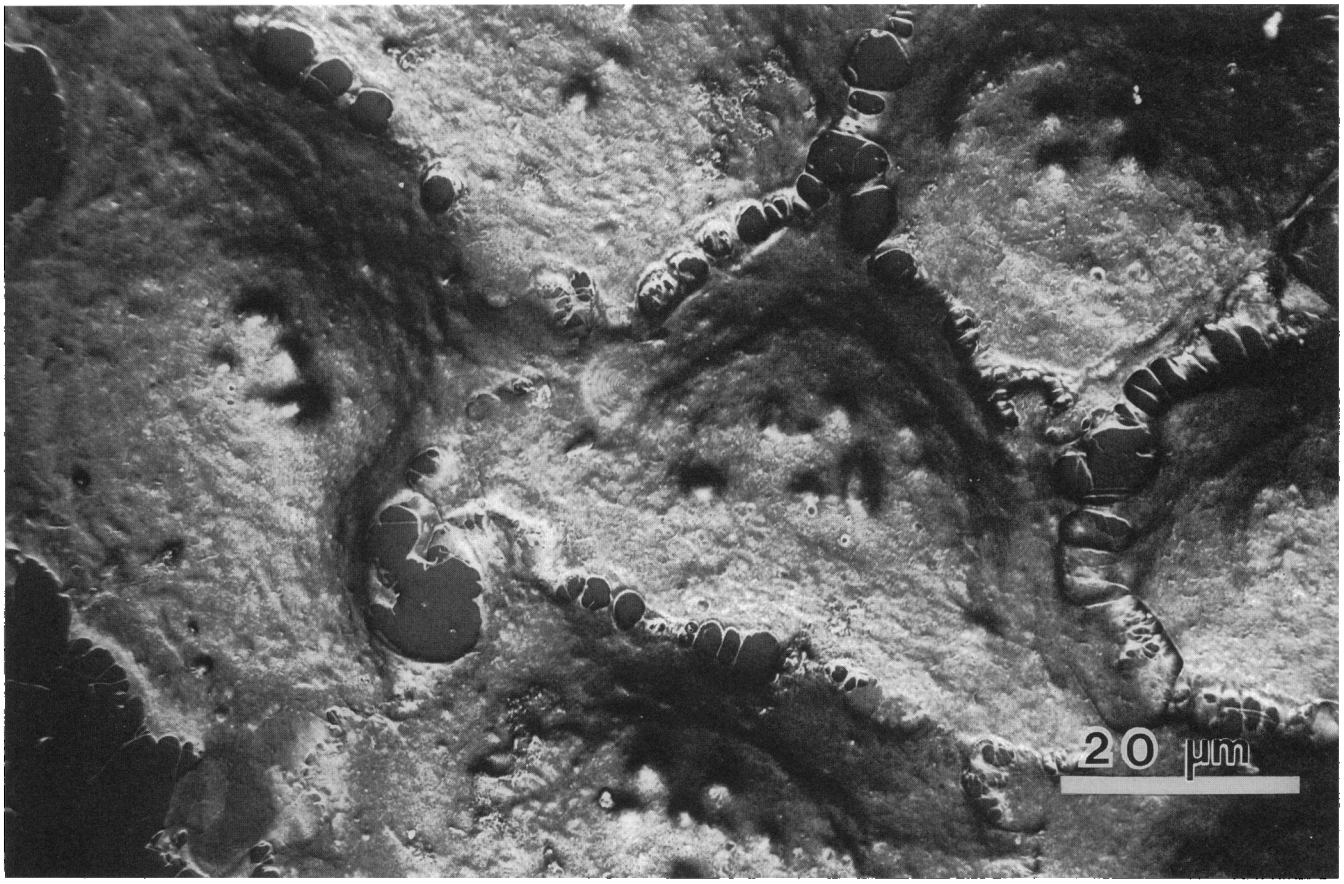


FIGURE 5 Optimized photoelectron micrograph of human breast carcinoma cells. The specimen is the same as in Fig. 3, but with a larger field of view, and the 50-$\mu$m aperture is positioned slightly off center to produce a three-dimensional effect (i.e., by enriching the image in electrons emitted from one side of each topographical feature, resulting in a shadowing effect). The micrograph was recorded with combined mercury arc lamp and laser illumination as in Fig. 3 *c*.

because these gaps are not observed in similarly treated normal epithelial cells.

## Photoelectron beam current data and optical absorption data

Additional insight into the role of photoconductivity can be obtained from the photoelectron beam current data. Table 1 lists representative emission currents from confluent monolayers of carcinoma and fibroblast cells. With only the short UV excitation source, the aperture stop blocks a larger fraction of the beam current emitted from the carcinomas than from the fibroblasts. This is most easily seen in the ratios of beam currents that get through to the image with the stop in and with the stop out (last column, Table 1). When photoconductivity is increased by switching on the laser, the fraction of the emission current from the carcinoma monolayers passing through the aperture increases, whereas there is little change in the corresponding ratio for fibroblast monolayers. The reason for this is that, when charging of the carcinoma specimen is eliminated, the electrons are no longer deflected through such large angles. The specimen charging, and discharging by the laser, occur rapidly, in less than 0.1 s, the speed of our mechanical shutter on the laser. There is often a small increase in the beam current when the laser is switched on. This is due to an increase in the photoemission by the laser, but this is a relatively small contribution compared to the emission caused by the short-wavelength mercury arc lamp. Over time the beam currents increase irreversibly and the charging effects eventually decrease. Time (UV dose)-dependent photoelectron quantum yields have been noted previously and are probably due to photochemistry taking place over the life of the experiment (Griffith et al., 1981).

The emission currents vary somewhat from specimen to specimen, because of the heterogeneous nature of cultured cell preparations. However, the beam currents (measured with no aperture present) are generally within an order of magnitude per unit area, whether or not charging is present. An emission current of $18 \times 10^{-11}$ A was measured from a specimen area of diameter 120 $\mu$m with the mercury arc lamp short UV illumination. This corresponds to a current density (J) of $1.6 \times 10^{-6}$ A/cm$^2$ at the specimen. Literature values of the resistivity of protein films are typically $\rho = 10^{12}$ ohm cm to $10^{13}$ ohm cm (Gutmann and Lyons, 1967).

**TABLE 1 Photoelectron emission currents from confluent monolayers of cells**

| Cell type | Illumination | −aperture | +aperture | +aperture/−aperture |
|---|---|---|---|---|
| Carcinoma | Hg arc | 0.8 | 0.04 | 0.05 |
| Carcinoma | Hg arc + laser | 2 | 0.2 | 0.1 |
| Fibroblast | Hg arc | 10 | 4 | 0.4 |
| Fibroblast | Hg arc + laser | 10 | 4 | 0.4 |

Representative data for monolayers of two cell lines; a carcinoma (MCF-7), and a fibroblast (Wi-38). The photoelectron images of the MCF-7 cells exhibited significant charging effects. The photoelectron images of Wi-38 exhibited little or no charging. The mercury arc lamp optics were adjusted for short-wavelength UV (254 nm). The Omnichrome laser produced 325 nm wavelength radiation. Photoelectron emission currents are in units of amperes (A) and are multiplied by $10^{11}$. Measurements were taken with (+) and without (−) the 50-$\mu$m diameter aperture stop. The beam currents were collected on an aluminum-coated phosphor below the projector lens of the photoelectron microscope 10 min after the UV light was switched on, with the electron lenses set for the imaging of cells.

Assuming $\rho = 10^{12}$ ohm cm and a cell thickness of 5 $\mu$m, one calculates a voltage across the thickness ($t$) of the cell as $V = IR = J\ \rho\ t = 800$ V. A surface potential of this magnitude would create a field (i.e., 800 V/5 $\mu$m = $1.6 \times 10^8$ V/m) much larger than the accelerating field. This would lead to deflections due to charging that are much larger than those observed (~10 milliradians) in the aperture plane of the microscope. These findings provide evidence that, for the experimental conditions in the present study, the conductivity of the specimen is greatly enhanced over what would be expected from the literature values of the resistivity.

Optical absorption data for a dried film, about 20 $\mu$m thick, of bovine serum albumin (BSA) and monolayers of MCF-7 and Wi-38 cells are shown in Fig. 6. The three wavelengths examined correspond to the UV short wavelength line of the Hg arc, 254 nm, and the two laser lines, 325 nm and 440 nm. The MCF-7 cells, when examined unfixed, absorb more strongly at all three wavelengths than the 20 $\mu$m film of BSA, suggesting that the thickness of these cancer cells is greater than 20 $\mu$m. Unfixed Wi-38 cells, on the other hand, exhibit substantially less absorption at 254 nm than the film of BSA, and these fibroblasts are thus apparently somewhat thinner. A monolayer of a third cell line, Balb/c 3T3 mouse fibroblasts, exhibited optical absorption that was intermediate between MCF-7 and Wi-38 (data not shown). When viewed under the microscope, the MCF-7 cancer cells appear to grow in dense clusters. The Wi-38 cells and Balb/c 3T3 fibroblasts grow to relatively uniform confluent monolayers. Once the cells are fixed for photoelectron microscopy, the optical absorption in both the UV and visible regions increases significantly for all three cell types. However, even under the most light-absorbing conditions (osmium tetroxide post-fixed MCF-7 cells), approximately 20% of the 325 nm light and 50% of the 440 nm light passes completely through the cells and reaches the substrate. The 254-nm light is much more strongly absorbed, and even this short UV light penetrates deep into the specimens, far beyond the plasma membrane, which is only about 10 nm thick.

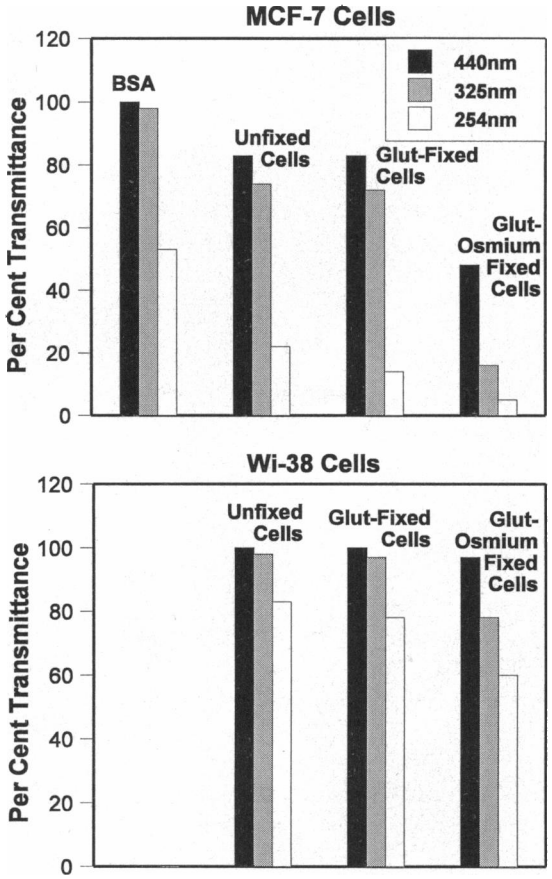


FIGURE 6 Percentage transmittance of a thin film of bovine serum albumin (BSA) and monolayers of MCF-7 human breast carcinoma cells (*top graph*) and Wi-38 normal human lung fibroblasts (*bottom graph*) measured at three wavelengths: 254 nm, 325 nm, and 440 nm. The samples were prepared on sapphire disks, which are transparent in the UV-visible region, and were examined during three stages of preparation for photoelectron microscopy; unfixed, glutaraldehyde-fixed (Glut-fixed), and glutaraldehyde-fixed cells postfixed with osmium tetroxide (Glut-Osmium fixed).

## DISCUSSION

### Photoemission from organic and biological surfaces

To understand the photoelectron imaging process it is useful to consider the escape depth of the photoelectrons and the effects of the electric field across the cathode-anode gap of the photoelectron microscope. Photoemission can be considered as a four-step process: 1) absorption of the UV light, 2) photoionization at a depth $z$ in the sample, 3) transport of the photoionized electrons to the surface ($z = 0$), and 4) escape from the surface into the vacuum. The number of photoelectrons originating between the depth $z$ and $z + dz$ that contribute to the total photoelectron quantum yield ($Y_d$, the number of electrons/incident photon) for a sample of thickness $d$ is the product of four independent probabilities. The probability of

the first step ($dP_1$) the absorption of light of energy $h\nu$ at a depth $z$ in a thickness $dz$, is given by the Beer-Lambert relation $P_1 = \alpha \exp(-\alpha z)dz$, where $\alpha$ is the optical absorption coefficient of the UV light. The probability of the second step ($P_2$) is the photoelectron quantum yield for the photoionization of an electron into the medium of dielectric constant $\epsilon$. This step is assumed to be independent of the depth $z$. The probability of the transport step ($P_3$) is a function of the energy ($E$) of the photoelectrons and the distance $z$, as given by the exponential relation $P_3 = \exp(-z/L)$, where $L$ is the electron attenuation length. In the fourth and last step, electrons reaching the surface must then overcome a surface potential to escape into the vacuum. The probabilities of the second and fourth steps are independent of $z$. Taking the product of the probabilities of these four steps, and integrating over the interval from the depth $z$ to $z = 0$, gives the expression for the total photoelectron quantum yield

$$Y_d = B\{1 - \exp[-(\alpha + 1/L)d]\} \quad (2)$$

where $d$ is the sample thickness and the factors $P_2$ and $P_4$, which are independent of $z$, are included in the coefficient $B$ (Burke et al., 1974; Sommer and Spicer, 1965). Eq. 2 defines a characteristic specimen depth: $d_o = (\alpha + 1/L)^{-1}$, from which about 63% (i.e., the fraction $1 - 1/e$) of the electrons escape. It is known from plots of $Y_d$ vs. $d$ that $L$ is very short for organic and biological macromolecules, typically 2 to 5 nm (Houle et al., 1982). Values of $\alpha$ depend on wavelength, but even for the most strongly absorbing UV light (254 nm), the optical transmission data of Fig. 6 indicate that $\alpha = 1.5 \times 10^2$ cm$^{-1}$ for the 20 $\mu$m uniform film of the reference protein, BSA, and about $3 \times 10^2$ cm$^{-1}$ for the most absorbing specimen, the glutaraldehyde/$OsO_4$ fixed MCF-7 cells. Thus for all of these specimens $1/L \gg \alpha$, the exponential term is small for typical specimen thicknesses, and $Y_d \approx B$, a constant. The light penetrates deep into the specimens, but only a thin layer, roughly the thickness of the cell membrane, acts as a photocathode. This is one reason why photoelectron microscopy produces sharp images of cell surfaces. Only electrons originating from this thin outer layer escape and contribute to the observed image.

## Photoelectron imaging: effect of the accelerating field

In the photoelectron microscope the specimen is mounted on the cathode and held at a high negative potential relative to the anode, so that the emitted electrons are accelerated before imaging in an electron lens system. The accelerating gap of the microscope used in this study is 4 mm and the accelerating voltage is 30,000 V. The accelerating field is $7.5 \times 10^6$ V/m and is directed along the microscope axis (the $z$ axis). Electrons emerge with very low energies and their trajectories are strongly influenced by the microfields at the surface of the specimen. Electrons emitted from flat areas of the specimen surface are undeflected as they leave the surface, and follow parabolic trajectories during acceleration in the cathode-anode gap. Electrons emitted from the sloping sides of protrusions are deflected by the altered electric field, causing them to pass through the objective aperture off-center. The net result is that the aperture blocks out proportionately more of the electrons emitted from the steep sides of an object. This is responsible for the excellent topographical contrast in the photoelectron images. Calculations have been performed on simplified models of surface relief to verify the topographical contrast mechanism (Rempfer et al., 1980). The main requirement is that the potential (i.e., microfields) at the surface must be due solely to topographic detail, and not spurious effects, as could be caused by specimen charging. When imaging artifacts are present, as in Figs. 2 *a* and 3 *a*, we find that the use of a second light source at longer wavelengths is able to convert a blurred or missing image into a sharp image. Thus, the initial problem must have been specimen charging. Consistent with this, when the carcinoma cells are coated with a thin layer of conductive metal, they are readily imaged (Fig. 4). Because the metal coating has very little effect on the topography, this result confirms that the topography is not causing the image distortions.

Both rounded tumor cells and flatter normal cells presumably have very similar photoelectron quantum yields (e.g., *emitted* beam currents), because the composition of the surfaces is similar. The high accelerating field across the cathode-anode gap ensures that all specimens, charging or not, will produce beam currents if the exciting light has sufficient energy to eject electrons. Without this accelerating field, a substantial retarding field could build up on the specimen surface, resulting in a decreasing emission current. Although sample charging produces dark regions in the images, this is largely due to deflection of the electrons and their removal by the aperture stop, rather than a failure of the affected region of the cell surface to emit electrons.

## A model for specimen charging in photoelectron imaging

Consider a thin, flat specimen on the cathode. Uncoated biological specimens are semiconductors, so that some currents, however small, do occur. When the voltage is applied, the specimen and anode act as plates of a capacitor; a negative charge is induced on the surface of the specimen, and a positive charge is induced on the anode. Before the UV light is turned on there is no emission, and the surface of the specimen rises to the potential of the cathode. The magnitudes of the induced charges per unit area are the same, $q_s = E_z\epsilon_o$, where $\epsilon_o$ is the dielectric constant of free space. The fields due to these surface charges add constructively in the space between the "capacitor plates" and cancel outside, leaving the interior of the specimen field-free. When the light is switched on, photoelectrons are emitted

from the surface layer of the specimen, and are replenished from the high-voltage power supply via the cathode. If the conductivity of the specimen is sufficient to replenish the electrons with only a negligible *IR* drop across the thickness of the specimen, the potential of the surface is not affected. If the conductivity is not sufficient, the *IR* drop will not be negligible, and the surface potential of the specimen will become positive relative to cathode potential. Charging effects have been widely studied in the related field of photoelectron spectroscopy (Cros, 1992; Sato et al., 1985; Koch, 1987; Gonska et al., 1977; Briggs and Seah, 1983; Salaneck and Zallen, 1976). The simplest case occurs when a uniform D.C. bias develops, so that Einstein's equation (Eq. 1) becomes

$$KE = h\nu - \phi - C \tag{3}$$

where $C$ is the steady-state bias due to charging. Positive D.C. charging of the emitting surface reduces the kinetic energy of the electrons at the spectrometer, and shifts the positions of the energy peaks, but does not preclude their determination.

In photoelectron microscopy, a uniform D.C. bias on the specimen surface would have the effect of simply shifting the plane of focus; it would not cause the image artifacts seen in Figs. 2 *a* and 3 *a*. However, if $C$ in Eq. 3 becomes $C_{x,y,t}$, i.e., if charging varies in time or from place to place on the specimen surface, the image can be adversely affected. Rapid variations in time would cause the focal distance to vary during recording of the image and would result in a fuzzy image. Nonuniform charging creates lateral fields that alter the *directions* of the electrons leaving the specimen, resulting in dark areas of the image. Another consequence of non-uniform charging is that not all parts of the image are in focus at the same focal setting. These last two effects of non-uniform charging are illustrated for the simple case of a flat specimen in Fig. 7. The effect of altering the trajectories of the electrons is particularly important where the specimen is not flat, i.e., where there is substantial specimen topography. It is expected that for a high-resistivity material the charging of the surface would be much greater for a thick region than for a thin region in contact with the substrate. Assume, for example, that in a

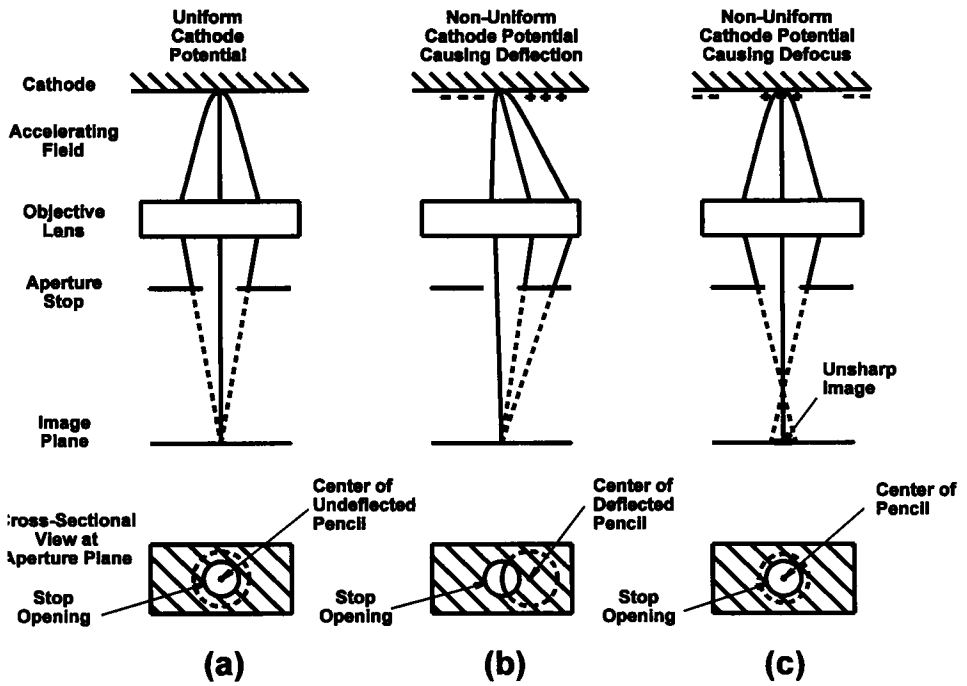


FIGURE 7 Schematic diagrams showing how specimen charging can alter the photoelectron image. In all three diagrams pencils of rays depart from the surface of a flat specimen at a point on the axis of the electron optical system. The specimen surface is at a high negative potential (i.e., the cathode). In (*a*) the specimen surface is at a uniform potential, and the ray pencil remains centered on the axis as the electrons follow their parabolic paths in the accelerating field and pass through an opening in the grounded anode (not shown) before reaching the objective lens. After the electrons pass through the objective lens, the pencil is on center at the aperture stop, and only the peripheral rays are kept from reaching the image. In (*b*) the specimen surface does not have a uniform potential, some areas being less negative than others, and the resulting transverse field causes a deflection of the ray pencil. The pencil is off center at the aperture stop, and a smaller fraction of the rays reach the image. This results in a darkened image of the charging regions. In diagram (*c*) the electrons are emitted from the center of a cylindrically symmetric charged region and the pencil of rays is not deflected. However, these electrons will focus in a plane nearer the lens, because the charge is positive with respect to cathode potential. This results in an unsharp image of the charged regions combined with a sharp, in-focus image of the uncharged regions of the specimen. In images of charging cells, these two effects combine to produce a dark area with an out-of-focus bright spot in the center. The drawing is not to scale. The (+) marks indicate regions with a small positive charge relative to rest of the cathode. All regions of the specimen are at a high negative potential with respect to the anode.

rounded-up cell the central region containing the nucleus is 5 $\mu$m thick, whereas in the peripheral region the cell may be only 0.5 $\mu$m thick. If the potential of the cell surface over the nucleus is +10 V with respect to cathode potential, and at a distance of 10 $\mu$m away, another region of the surface is uncharged, the average electric field between these points is 1 V/$\mu$m. This lateral field due to charging is appreciable compared with the accelerating field ($7.5 \times 10^6$ V/m = 7.5 V/$\mu$m) and can produce a significant deflection of the electrons emitted from the specimen between the center of the charged area and the periphery, causing them to miss the hole in the aperture stop. To illustrate, the aperture stop in the present experiments has a diameter of 50 $\mu$m and is located in the exit-pupil plane of the objective lens. The focal length of the objective lens is $f_1$ = 10 mm. If electrons pick up 3 eV of energy associated with lateral motion, their trajectories will make an angle $\alpha_a$ of $[3 \text{ eV}/(3 \times 10^4 \text{ eV})]^{1/2}$ = 10 milliradians (mr) with the optical axis after acceleration through 30 kV. In addition, the diverging effect of the anode aperture increases this angle by the factor 3/2 to $\alpha_1$ = 15 mr. The electrons strike the aperture stop at a distance from the axis of $\rho_A \cong \alpha_1 f_1 = (0.015)(10 \text{ mm}) = 150$ $\mu$m, six times the radius of the 50-$\mu$m aperture (for a discussion of the optics of PEM, see Griffith and Rempfer, 1987; Rempfer and Griffith, 1989). The maximum $\alpha_1$ transmitted by the aperture is only about 2.5 mr, corresponding to a lateral energy of less than 0.1 eV; electrons deflected by more than 2.5 mr therefore do not reach the image. We have been able to observe the large-angle beams from charged specimens by focusing the intermediate lens on the aperture plane and withdrawing the aperture stop. We have also measured the current in the image with and without the aperture stop in place and found that the ratio of the current with stop to that without stop is considerably smaller when the cells are charged than when they are uncharged (Table 1).

Since the charged area of a cell has a positive potential relative to the surrounding surface, electrons are deflected toward the center of the area. Most of these electrons have large enough deflections to be intercepted by the aperture stop. However, electrons emitted close to the center are not deflected as much. Some of these electrons pass through the aperture stop and reach the image plane. The image they produce is out of focus because of chromatic aberration and appears as a bright spot. This explains the bright, unfocused centers surrounded by black regions in the images of severely charged cells of Fig. 3 *a*.

## Photoconductivity

Photoconductivity of dehydrated cells has evidently not been examined previously, but photoconductivity of organic layers has been extensively studied because of its importance in xerography and related fields (Mort, 1989; Borsenberger and Weiss, 1993).

The conductivity ($\sigma$) of the specimen is given by the well-known equation

$$\sigma = nq\mu \quad (4)$$

where $n$ is the number of charge carriers, $q$ is the charge on each carrier, and $\mu$ is the mobility of the carrier (i.e., the carrier velocity per unit applied electric field). The change of conductivity $\Delta\sigma$ with illumination is, from Eq. 4, $\Delta\sigma = \Delta nq\mu$, where it is assumed for simplicity that one type of carrier predominates, and the main effect is the increase in the number of carriers. In the present experiments two different light sources are used, either separately or together. The first source provides short-wavelength illumination, typically 254 nm UV light. The 254 nm light has two effects: it is the major excitation source for the external photoelectron emission responsible for producing the image; it also produces internal photoelectrons, which become additional carriers $\Delta n_1$ and increase the conductivity. The second source provides light of longer wavelength, approximately 325 nm. This source produces very little external photoelectron emission; its main effect is to produce additional carriers $\Delta n_2$, which further increase the conductivity. For a broad range of biological specimens, including DNA, viruses, and many well-spread cells, the intrinsic conductivity and the photoconductivity accompanying the short UV irradiation combined are sufficient to produce excellent photoelectron images. However, in specimens where charging occurs it is clear from the parameters in Eq. 2 for the photoelectron yield why increasing the flux of photons in the short UV range (254 nm) cannot solve the problem. The short UV photons deplete the charge in the surface layer at a rate greater than or equal to the increase in photoconduction. Increasing the flux of photons in the short UV range will increase the charge depletion and the photoconductivity proportionately. The success of the longer wavelength (e.g., 325 nm) radiation in abolishing charging artifacts is due to the fact that, at this wavelength, the quantum yield for production of external photoelectrons from proteins and polysaccharides is much lower than for the short wavelength radiation (Griffith et al., 1981), so that the combined increase in number of carriers $\Delta n = \Delta n_1 + \Delta n_2$ can neutralize the charge distribution at the surface. Both the photoconductivity produced by the mercury arc lamp, alone or with the laser, and the effect of the accelerating field, which penetrates into the specimen to some extent during emission, contribute to the increase in conductivity. Furthermore, because a significant fraction of the long wavelength light (325 nm or 440 nm) passes through the specimen, charge injection from the metal substrate may contribute to the increase in conductivity.

## SUMMARY

Uncoated biological specimens are inherently poor conductors. The success of photoelectron microscopy is explained in part by the enhanced conductivity induced by the UV light and the electric field across the specimen. To analyze the process, the specimen is divided into two regions; the outermost layer acts as a photocathode, transforming the

incoming beam of UV light into an information-carrying electron beam. The underlying bulk specimen provides a conduction path from the metallic substrate to the surface. For most specimens, such as DNA-protein complexes, viruses, and many well-spread cells, the conventional arrangement of one UV lamp is sufficient. However, certain classes of rounded-up cells, including many cancer cell lines, exhibit charging. The specimen charging can be greatly reduced or eliminated by simultaneously flooding the specimen with light of longer wavelength. The long-wavelength light replenishes charge carriers at the surface by enhancing photoconduction in the bulk specimen, and very likely also charge injection from the metallic substrate, without contributing to the depletion of charge carriers at the surface.

We are pleased to acknowledge useful discussions with Drs. Wilfried Engel and Joseph Mort. We thank Walter P. Skoczylas and Denis Desloge for technical assistance. This work was funded by PHS grant CA11695 from the National Cancer Institute.

## REFERENCES

Birrell, G. B., D. L. Habliston, and O. H. Griffith. 1994. Photoelectron imaging of viruses and DNA: Evaluation of substrates by unidirectional low angle shadowing and photoemission current measurements. *Biophys. J.* 67:2041–2047.

Birrell, G. B., K. K. Hedberg, D. L. Habliston, and O. H. Griffith. 1991. Biological applications of photoelectron imaging: a practical perspective. *Ultramicroscopy.* 36:235–251.

Borsenberger, P. M., and D. S. Weiss. 1993. Organic photoreceptors for imaging systems. Marcel Dekker, New York. 447 pp.

Briggs, D., and M. P. Seah, editors. 1983. Practical surface analysis by Auger and x-ray photoelectron spectroscopy. John Wiley & Sons, New York.

Burke, C. A., G. B. Birrell, G. H. Lesch, and O. H. Griffith. 1974. Depth resolution in photoelectron microscopy of organic surfaces. The photoelectric effect of phthalocyanine thin films. *Photochem. Photobiol.* 19:29–34.

Clark, E. A., and J. S. Brugge. 1995. Integrins and signal transduction pathways: the road taken. *Science.* 268:233–239.

Cros, A. 1992. Charging effects in x-ray photoelectron spectroscopy. *J. Elect. Spectrosc. Rel. Phen.* 59:1–14.

Danø, K., N. Behrendt, N. Brünner, V. Ellis, M. Plough, and C. Pyke. 1994. *Fibrinolysis.* 8(Suppl. 1):189–203.

De Stasio, G., and G. Margaritondo. 1994. Photoemission spectromicroscopy. *In* New Directions in Research with Third-Generation Soft X-Ray Synchrotron Radiation Sources. A. S. Schlachter and F. J. Wuilleumier, editors. Kluwer Academic Publishers, The Netherlands. NATO ASI Ser. Ser. E, 254. 299–313.

Gonska, H., H. J. Freund, and G. Hohlneicher. 1977. On the importance of photoconduction in ESCA experiments. *J. Elect. Spectrosc. Rel. Phen.* 12:435–441.

Griffith, O. H., and W. Engel, editors. 1991. Proceedings of the Second International Symposium and Workshop on Emission Microscopy and Related Techniques (Part of the XII International Congress for Electron Microscopy), Seattle, Washington, 16–17 August, 1990. *Ultramicroscopy.* 36. 274 pp.

Griffith, O. H., D. L. Holmbo, D. L. Habliston, and K. K. Nadakavukaren. 1981. Contrast effects in photoelectron microscopy. UV dose-dependent quantum yields of biological surface components. *Ultramicroscopy.* 6:149–156.

Griffith, O. H., and G. F. Rempfer. 1987. Photoelectron imaging: photoelectron microscopy and related techniques. *In* Advances in Optical and Electron Microscopy, Vol. 10. R. Barer and V. E. Cosslett, editors. Academic Press, London. 269–337.

Gutmann, F., and L. E. Lyons. 1967. Organic Semiconductors. John Wiley and Sons, Inc., New York. 758–765.

Habliston, D. L., G. B. Birrell, K. K. Hedberg, and O. H. Griffith. 1986. Early phorbol ester induced release of cell surface fibronectin: direct observation by photoelectron microscopy. *Eur. J. Cell Biol.* 41:222–229.

Hedberg, K. K., G. B. Birrell, P. L. Mobley, and O. H. Griffith. 1994. The transition metal chelator TPEN counteracts phorbol ester-induced actin cytoskeletal disruption in C6 rat glioma cells without inhibiting activation or translocation of protein kinase C. *J. Cell. Phys.* 158:337–346.

Holldack, K., and M. Grunze. 1994. Recent advances in x-ray photoelectron microscopy. *Anal. Chim. Acta.* 297:125–138.

Houle, W. A., W. Engel, F. Willig, G. F. Rempfer, and O. H. Griffith. 1982. Depth of information in photoelectron microscopy. *Ultramicroscopy.* 7:371–380.

Koch, E.-E. 1987. Photoemission from organic molecular solids and organometallic compounds. *Phys. Scripta.* T17:120–136.

Massey, G. A., T. J. Ash, and H. Zhou. 1991. Nonlinear organic photoemitters: their properties and possible applications in electron microscopy. *Ultramicroscopy.* 36:186–195.

Mort, J. 1989. The Anatomy of Xerography, Its Invention and Evolution. McFarland and Company, Inc., North Carolina. 226 pp.

Rempfer, G. F., and O. H. Griffith. 1989. The resolution of photoelectron microscopes with UV, x-ray, and synchrotron excitation sources. *Ultramicroscopy.* 27:273–300.

Rempfer, G. F., and O. H. Griffith. 1992. Emission microscopy and related techniques: resolution in photoelectron microscopy, low energy electron microscopy and mirror electron microscopy. *Ultramicroscopy.* 47:35–54.

Rempfer, G. F., K. K. Nadakavukaren, and O. H. Griffith. 1980. Topographical effects in emission microscopy. *Ultramicroscopy.* 5:437–448.

Rempfer, G. F., W. P. Skoczylas, and O. H. Griffith. 1991. Design and performance of a high-resolution photoelectron microscope. *Ultramicroscopy.* 36:196–221.

Ryan, K. P. 1992. Cryofixation of tissues for electron microscopy: A review of plunge cooling methods. *Scanning Microsc.* 6:715–743.

Salaneck, W. R., and R. Zallen. 1976. Surface charging effects on valence band spectra in x-ray photoemission: crystalline and amorphous $As_2S_3$. *Solid State Commun.* 20:793–797.

Sato, N., H. Inokuchi, B. M. Schmid, and N. Karl. 1985. Ultraviolet photoemission spectra of organic single crystals. *J. Chem. Phys.* 83: 5413–5419.

Sheetz, M. P. 1995. Cellular plasma membrane domains. *Mol. Membr. Biol.* 12:89–91.

Sommer, A. H., and W. E. Spicer. 1965. Photoelectric emission. *In* Photoelectronic Materials and Devices. S. Larach, editor. D. van Nostrand, New York. 177–179.

Tonner, B. P., and G. R. Harp. 1988. Photoelectron microscopy with synchrotron radiation. *Rev. Sci. Instrum.* 59:853–858.